Raman-Induced Timing Jitter in Dispersion-Managed Optical Communication Systems

Jayanthi Santhanam and Govind P. Agrawal, *Fellow, IEEE*

***Abstract*—The moment method is used to calculate the Raman-induced timing jitter generated by amplifier-induced fluctuations in the energy, frequency, and position of optical pulses propagating inside dispersion-managed fiber links. Using a Gaussian form for chirped optical pulses in combination with the variational analysis, we obtain an analytic expression for the timing jitter whose predictions agree well with the numerical results obtained by solving the nonlinear Schrödinger equation directly. The effects of third-order dispersion are also included in the analysis. We also apply the moment method to standard solitons propagating inside dispersion-decreasing fiber as well as to chirped return-to-zero (CRZ) lightwave systems. We apply our results to a specific 160-Gb/s system and find that the Raman jitter resulting from intrapulse Raman scattering limits the transmission distance in all three cases.**

***Index Terms*—Dispersion management, optical fiber communication, optical solitons, Raman scattering, timing jitter.**

I. Introduction

MODERN dispersion-managed lightwave systems are limited mainly by the nonlinear effects occurring inside optical fibers and by the amplified spontaneous emission (ASE) added at the amplifiers [1]–[3]. Optical solitons can solve the first problem to some extent since they use the self-phase modulation (SPM), a dominant nonlinear mechanism, to balance the residual dispersion [4]. However, the ASE noise remains a serious limitation of soliton systems; it manifests through a reduced signal-to-noise ratio and an increased timing jitter at the optical receiver [2]. At bit rates of up to 10 Gb/s or so, timing jitter results mostly from the Gordon–Haus (GH) effect that has its origin in ASE-induced frequency fluctuations [5]. However, at higher bit rates for which the pulsewidth becomes shorter than 5 ps, the Raman-induced timing jitter is likely to become the most limiting factor. The origin of Raman jitter lies in intrapulse Raman scattering [4], a phenomenon responsible for the soliton self-frequency shift (SSFS) and occurring for short optical pulses whose spectrum is wide enough that its high-frequency components can amplify the low-frequency components of the same pulse through the Raman effect [6].

Manuscript received January 10, 2002; revised March 14, 2002. This work was supported in part by the National Science Foundation under Grant ECS-9903580 and Grant DMS-0073923.

J. Santhanam is with the Department of Physics and Astronomy, University of Rochester, Rochester, NY 14627 USA.

G. P. Agrawal is with The Institute of Optics, University of Rochester, Rochester, NY 14627 USA and also with the Department of Physics and Astronomy and the Laboratory for Laser Energetics, University of Rochester, Rochester, NY 14627 USA.

Publisher Item Identifier S 1077-260X(02)05472-2.

The Raman jitter occurs for both soliton and nonsoliton systems and results from the following sequence of events. Fluctuations in the pulse energy induced by the ASE noise at the location of lumped optical amplifiers are converted into frequency fluctuations through intrapulse Raman scattering, which are in turn translated into timing jitter by the group-velocity dispersion (GVD). The Raman jitter has been studied in the context of constant-dispersion fibers [7] as well as dispersion-decreasing fibers (DDFs)[8]. However, most lightwave systems make use of dispersion management. In this paper, we consider the impact of Raman-induced timing jitter on dispersion-managed (DM) systems and show that such systems are inherently limited by it at bit rates of 80 Gb/s or more. Our approach is based on an extension of the moment method that has been applied recently to calculating the GH jitter in dispersion-managed systems [9]–[12]. This approach allows us to obtain the analytic expressions for the timing jitter even when the contributions of both the intrapulse Raman scattering and third-order dispersion (TOD) are included.

The paper is organized as follows. We present in Section II the relevant details of the moment method and show in Section III how this method provides a simple expression for the Raman-induced frequency shift in DM systems. In Section IV, we obtain an analytic expression for the timing jitter by focusing on the case of DM solitons. The same technique is used in Section V for standard solitons propagating inside DDFs. Section VI is devoted to quasilinear CRZ systems. In Section VII, we compare our analytical results with the numerical simulations and apply them for calculating the timing jitter for a specific lightwave system designed to operate at a bit rate of 160 Gb/s. The main conclusions are summarized in Section VIII.

II. Moment Method

A typical DM system consists of a periodic sequence of anomalous- and normal-dispersion fibers. An optical amplifier is inserted for compensating fiber losses after one or several map periods. Each amplifier restores pulse energy to its original input value, but at the same time, adds the spontaneous-emission noise. This noise perturbs each optical pulse such that its amplitude, width, position, frequency, and phase all vary in a random fashion along the fiber link. Frequency fluctuations affect the pulse position because of dispersion and lead to the GH jitter [5]. Although amplitude fluctuations are believed not to contribute to the timing jitter, we show in this paper that they introduce considerable jitter when intrapulse Raman scattering becomes important.

Propagation of short optical pulses inside optical fibers is governed by the following nonlinear Schrödinger (NLS) equation generalized to include the Raman contribution [4]

$$i\frac{\partial A}{\partial z}-\frac{\beta_2}{2}\frac{\partial^2 A}{\partial t^2}-i\frac{\beta_3}{6}\frac{\partial^3 A}{\partial t^3}+\gamma|A|^2A = -\frac{i\alpha}{2}A+T_R\gamma A\frac{\partial|A|^2}{\partial t} \quad (1)$$

where $A(z,t)$ is the slowly varying amplitude of the pulse envelope, α accounts for fiber losses, β_2 is the GVD coefficient, β_3 is the TOD parameter, γ is the nonlinear parameter responsible for SPM, and the Raman parameter T_R accounts for the SSFS effect. Equation (1) cannot be solved analytically because the parameters α, β_2, β_3, and γ are not constants, but vary along the fiber link in a periodic fashion. Approximate solutions can be obtained using a variational technique and are found to be reasonably accurate through numerical simulations [13]–[15].

In the variational technique, each chirped Gaussian pulse launched initially is assumed to maintain its shape approximately, and the optical field is written as

$$A(z,t)=a\exp\left[-\frac{(1+iC)(t-T)^2}{2\tau^2}+i\phi-i\Omega(t-T)\right] \quad (2)$$

where the amplitude a, phase ϕ, frequency Ω, time delay T, chirp C, and width τ all are functions of z. The use of variational method shows that the pulsewidth τ and chirp C evolve with z and satisfy the following set of two equations [13]–[15]

$$\frac{d\tau}{dz}=\frac{\beta_2 C}{\tau} \quad (3)$$

$$\frac{dC}{dz}=\frac{\beta_2(1+C^2)}{\tau^2}+\frac{\gamma a^2}{\sqrt{2}}. \quad (4)$$

The amplitude a can be related to the pulse energy through $E(z)=\int_{-\infty}^{\infty}|A|^2dt=\sqrt{\pi}a^2\tau$. The phase equation is not given here because the z dependence of phase plays no role in our analysis.

In the absence of the ASE and the Raman effect, the shift T in the pulse position and the frequency shift Ω both are zero in (2). The moment method introduces the following two moments for calculating them [9]

$$T=\frac{1}{E}\int_{-\infty}^{\infty}t|A|^2dt \quad (5)$$

$$\Omega=\frac{i}{2E}\int_{-\infty}^{\infty}(A^*A_t-AA_t^*)dt \quad (6)$$

where the subscript t denotes a time derivative. We use (1)–(6) to find that E, T, and Ω evolve along the fiber link as

$$\frac{dE}{dz}=-\alpha E+\sum_i(g_iE+\delta E_i)\delta(z-z_i) \quad (7)$$

$$\frac{d\Omega}{dz}=-\frac{T_R\gamma E}{2\sqrt{\pi}\tau^3}+\sum_i\delta\Omega_i\delta(z-z_i) \quad (8)$$

$$\frac{dT}{dz}=\beta_2\Omega+\frac{\beta_3(1+C^2)}{12\tau^2}+\beta_3\frac{\Omega^2}{6}+\sum_i\delta T_i\delta(z-z_i) \quad (9)$$

where the last term has been added phenomenological to account for the effects of lumped amplifiers. More specifically, g_i is the gain and δE_i, $\delta\Omega_i$, and δT_i are random fluctuations in the pulse energy, frequency, and position, respectively, introduced by the ith amplifier located at a distance z_i. The amplifier gain is chosen such that it compensates for all fiber losses accumulated up to that point. As a result, pulse energy decreases exponentially as $E_0\exp[-\alpha(z-z_i)]$ and recovers its input value E_0 at the next amplifier.

The Raman-induced frequency shift appears in (8) through the first term while the second term includes frequency fluctuations induced by ASE. Equation (9) shows that the pulse position changes in a deterministic fashion both by SSFS and TOD. Deterministic changes in soliton frequency and position are not of concern as they do not produce any timing jitter. However, if the pulse energy fluctuates because of ASE noise, the SSFS develops a random part which leads to jitter. This is the physical origin of the Raman jitter. More specifically, ASE-induced amplitude fluctuations are converted into timing jitter by the phenomenon of intrapulse Raman scattering.

The timing jitter induced by both Raman and GH effects can be calculated using $\sigma_t^2=\langle T^2\rangle-\langle T\rangle^2$, where the angle brackets indicate average over the ASE noise. For this purpose, we need the second moments of δE_i, $\delta\Omega_i$, and δT_i at every amplifier. These moments can be calculated using

$$\langle\delta A_i^*(t)\delta A_j(t')\rangle=S\delta_{ij}\delta(t-t') \quad (10)$$

where δA_i is the change in the optical field from its average value (i.e, $\langle\delta A_i\rangle=0$) at the ith amplifier, $S=n_{sp}h\nu(G-1)$ is the ASE spectral density of for an amplifier with gain G [3], n_{sp} is the spontaneous-emission factor related to the noise figure as $F_n=2n_{sp}$, and $h\nu$ is the photon energy. The two delta functions account for the fact that the each spontaneous-emission event is independent of all others.

Using (2)–(6) with (10), we obtain the following expressions for the variances and cross correlations of the three fluctuations δE_i, $\delta\Omega_i$, and δT_i

$$\langle\delta E_i^2\rangle=2SE_i,\quad \langle\delta\Omega_i\delta E_i\rangle=\frac{2SC_i}{\sqrt{\pi}\tau_i} \quad (11)$$

$$\langle\delta\Omega_i^2\rangle=\frac{S\left(1+C_i^2\right)}{E_i\tau_i^2},\quad \langle\delta E_i\delta T_i\rangle=0 \quad (12)$$

$$\langle\delta T_i^2\rangle=\frac{S\tau_i^2}{E_i},\quad \langle\delta\Omega_i\delta T_i\rangle=\frac{SC_i}{E_i} \quad (13)$$

where E_i, τ_i, and C_i are the energy, width, and chirp of the pulse at the output of the ith amplifier. For a soliton-based system, the pulse recovers its input parameters at each amplifier if we assume that the map period L_m is an integer multiple of the amplifier spacing L_A. This feature simplifies the timing-jitter calculation considerably for solitons.

III. Raman-Induced Frequency Shift

Along the fiber link E, Ω, and T evolve as dictated by (7)–(9) in a periodic fashion. It is useful to consider the first fiber section of length L_A and integrate these equations to find E, Ω, and T just before the first amplifier. Since the noise terms in these

equations can be set to zero, their solution is relatively simple and is given by

$$E(L_A) = p(L_A)E(0) \tag{14}$$

$$\Omega(L_A) = \Omega(0) + b_R E(0) \tag{15}$$

$$T(L_A) = T(0) + b_2\Omega(0) + b_{2R}E(0) + b_3 + b_{3\Omega}\Omega^2(0) + b_{E\Omega}E(0)\Omega(0) + b_{3E}E^2(0) \tag{16}$$

where $p(z) = \exp\left[-\int_0^z \alpha(z)dz\right]$ represents the power-reduction factor at a distance z. All new parameters involve integration over the amplifier spacing and are defined as

$$b_2 = \int_0^{L_A} \beta_2(z)dz, \quad b_3 = \int_0^{L_A} \frac{\beta_3(1+C^2)}{12\tau^2}dz \tag{17}$$

$$b_R = -\int_0^{L_A} q(z)dz, \quad b_{3\Omega} = \frac{1}{6}\int_0^{L_A} \beta_3 dz$$

$$b_{2R} = -\int_0^{L_A} dz\beta_2(z)\int_0^z dz' q(z') \tag{18}$$

$$b_{E\Omega} = -\frac{1}{6}\int_0^{L_A} dz\beta_3(z)\int_0^z q(z')dz' \tag{19}$$

$$b_{3E} = -\frac{1}{6}\int_0^{L_A} dz\beta_3(z)\left[\int_0^z q(z')dz'\right]^2$$

$$q(z) = \frac{T_R\gamma(z)p(z)}{2\sqrt{\pi}\tau^3(z)}. \tag{20}$$

Note that several parameters involve local values of the pulse width and chirp within the map period. These can be obtained by solving the variational (3) and (4).

The Raman-induced frequency shift is governed by (15) and depends on the pulse energy and the parameter b_R given in (18). In the case of constant-dispersion fibers and ideal distributed amplification ($\alpha = 0$), the pulsewidth remains constant, and the integral in this equation can be carried out analytically. Using $\Omega(0) = 0$, the frequency shift at a distance z is given by

$$\Omega(z) = -\frac{T_R\gamma E(0)}{4\sqrt{\pi}\tau_0^3}z = -\frac{T_R|\beta_2|}{2\tau_0^4}z \tag{21}$$

where we used $E(0) = \sqrt{\pi}P_0\tau_0$ together with $P_0 = |\beta_2|/\left(\gamma\tau_0^2\right)$ for fundamental solitons. This equation shows that the Raman-induced frequency shift scales with the pulsewidth as τ_0^{-4}, a result first derived in 1986 for standard solitons [6]. The factor of 1/2 appears in place of 8/15 because the pulse shape has been assumed to be Gaussian in deriving (21).

In the case of DM solitons, the situation is quite different. First, the pulsewidth τ is not constant but varies in a periodic fashion along the fiber link. It takes its minimum value in the middle of each fiber section forming the dispersion map. As a result, the maximum contribution to the integral in (18) comes from this region. It is sometimes concluded that SSFS is smaller for DM solitons if we assume that τ_0 in (21) corresponds to the minimum width of a DM soliton [16]. However, one should note that the pulse energy $E(0)$ is enhanced considerably for DM solitons. Moreover, the contribution where the pulsewidth is minimum is reduced because of losses. For these reasons, the Raman-induced frequency shift of DM solitons can exceed that of standard solitons.

IV. Timing Jitter for DM Solitons

We now consider the entire fiber link and include the effects of amplifier noise as well. Denoting by the subscript i the value of E, Ω, and T at the end of the ith amplifier and adding the fluctuations produced by that amplifier, we obtain the following simple recurrence relations from (14)–(16)

$$E_i = E_{i-1} + \delta E_i \tag{22}$$

$$\Omega_i = \Omega_{i-1} + b_R E_{i-1} + \delta\Omega_i, \tag{23}$$

$$T_i = T_{i-1} + b_2\Omega_{i-1} + b_{2R}E_{i-1} + b_3 + \delta T_i. \tag{24}$$

where, for simplicity, we have neglected the contribution of higher order terms in (24) containing $b_{3\Omega}$, b_{3E}, and $b_{\Omega E}$. These terms involve the product of two small parameters and can be neglected in most case of practical interest. The dominant contribution of the TOD effects is still included in the analysis through the b_3 term.

The recurrence relations in (22)–(24) can be solved for a chain of N amplifiers; we refer to [11] for details. The important quantity we need is the total temporal shift T_N of the pulse at the end of N amplifiers. Of course, when calculating T_N, we also need Ω_i and E_i at intermediate amplifiers as seen from (24). The net result is that T_N involves, single, double, and triple sums over N. When these sums are carried out, the average temporal shift at the end of Nth amplifier is given by

$$\langle T_N\rangle = \frac{b_2 b_R}{6}SN(N-1)(N-2) + \frac{1}{2}[b_{2R}S + b_2 b_R E_0]N(N-1) + (b_3 + b_{2R}E_0)N \tag{25}$$

where E_0 is the input pulse energy.

To calculate the Timing jitter σ_t^2 after N amplifiers, we also need the second moment $\langle T_N^2\rangle$. As seen from (24), its evaluation requires the variances and cross correlations of E_N, Ω_N, and T_N all of which can be obtained with the help of (11)–(13). After considerable algebra, we obtain the following analytic expression for the timing jitter:

$$\sigma_t^2 = \sigma_{\rm GH}^2 + R_1\langle(\delta E)^2\rangle + R_2\langle\delta E\delta\Omega\rangle + \frac{R_3 S}{E} \tag{26}$$

where $\sigma_{\rm GH}$ is the GH contribution to timing jitter and is given by

$$\sigma_{\rm GH}^2 = \frac{b_2^2}{6}N(N-1)(2N-1)\langle\delta\Omega^2\rangle + b_2 N(N-1)\langle\delta\Omega\delta T\rangle + N\langle\delta T^2\rangle \tag{27}$$

and the quantities R_1, R_2, and R_3 are defined as

$$R_1 = N(N-1)\times\left[\frac{b_R^2 b_2^2}{120}(N^3 - 10N^2 + 29N - 9) + \frac{b_2 b_R b_{2R}}{96}(19N^2 - 65N + 48) + \frac{b_{2R}^2}{6}(2N-1)\right] \tag{28}$$

$$R_2 = N(N-1)b_2\times\left[\frac{b_2 b_R}{12}(N-2)(3N-1) + \frac{b_{2R}}{3}(2N-1)\right] \tag{29}$$

$$R_3 = N(N-1)b_3\left[\frac{b_3}{6}(N-1)(N-2) + \frac{4b_2}{3\tau_0}(N-1)\right]. \tag{30}$$

The R_1 and R_2 terms originate from the Raman-induced frequency shift. For this reason, their contribution is referred to as the Raman jitter in this paper. The R_1 dominates in practice for $N \gg 1$ because of its N^5 dependence. The R_3 term results from the TOD effects and becomes quite important for pulses much shorter than 1 ps. In the absence of the Raman and TOD effects, we recover the expression for the GH jitter obtained in our earlier paper [10].

V. Timing Jitter for Standard Solitons

The preceding analysis of timing jitter is for DM solitons. The use of standard unchirped solitons requires propagation inside DDFs to ensure that the soliton shape and width is preserved in spite of fiber losses [8]. In DDFs, the dispersion decreases at a rate that matches the power loss. The GVD coefficient of such fibers decreases exponentially as $\beta_2(z) = \beta_2(0)\exp(-\alpha z)$ and reaches a value $\beta_2^{\min}$ at the end of each DDF section.

We can use the moment method for standard solitons provided we use a pulse shape of the form

$$A = a\,\mathrm{sech}\left(\frac{t}{\tau}\right)\exp[i\phi - i\Omega t]. \tag{31}$$

Note that the chirp parameter does not appear for standard solitons. Its absence simplifies the analysis considerably. One consequence of the absence of the chirp is that all cross correlations among δE_i, $\delta\Omega_i$, and δT_i vanish at every amplifier. More specifically, the variances and cross correlations at the ith amplifier are given by

$$\left\langle \delta E_i^2 \right\rangle = 2SE_0, \quad \langle \delta\Omega_i \delta E_i \rangle = 0 \tag{32}$$

$$\left\langle \delta\Omega_i^2 \right\rangle = \frac{2S}{3E_0\tau_0^2}, \quad \langle \delta E_i \delta T_i \rangle = 0 \tag{33}$$

$$\left\langle \delta T_i^2 \right\rangle = \frac{\pi^2 S\tau_0^2}{6E_0}, \quad \langle \delta\Omega_i \delta T_i \rangle = 0. \tag{34}$$

The Raman-induced frequency shift is also affected by the change in the soliton shape. In fact, (7)–(9) are replaced with

$$\frac{dE}{dz} = -\alpha E + \sum_i (g_i E + \delta E_i)\delta(z - z_i) \tag{35}$$

$$\frac{d\Omega}{dz} = -\frac{4T_R\gamma E}{15\tau^3} + \sum_i \delta\Omega_i \delta(z - z_i) \tag{36}$$

$$\frac{dT}{dz} = \beta_2\Omega + \frac{\beta_3}{18\tau^2} + \beta_3\frac{\Omega^2}{6} + \sum_i \delta T_i \delta(z - z_i). \tag{37}$$

In each fiber section of length L_A between two amplifiers, we can set the noise terms to zero. The integration is then straight forward. In fact, (14)–(16) remain unchanged but the coefficients are modified and are given by

$$b_2 = \beta_2(0)L_{\text{eff}}, \quad b_3 = \frac{\beta_3(0)L_{\text{eff}}}{(18\tau_0^2)} \tag{38}$$

$$b_R = -\frac{4\gamma T_R L_{\text{eff}}}{(15\tau_0^3)} \tag{39}$$

$$b_{2R} = -\frac{2\gamma T_R \beta_2(0) L_{\text{eff}}^2}{(15\tau_0^3)} \tag{40}$$

where L_{eff} is the effective length defined as

$$L_{\text{eff}} = \frac{[1 - \exp(-\alpha L_A)]}{\alpha}. \tag{41}$$

As before, we neglect the coefficients $b_{3\Omega}$, b_{3E} and $b_{E\Omega}$.

The variance of timing jitter can now be calculated analytically following the same method as before and is given by

$$\sigma_t^2 = \sigma_{\text{GH}}^2 + R_1\left\langle (\delta E)^2 \right\rangle + \frac{R_3 S}{E}. \tag{42}$$

A comparison of (26) and (42) show that the only difference is the absence of the R_2 term and different definitions of the parameters b_R, b_2 and b_{2R}. The GH contribution is also different and is given by

$$\sigma_{\text{GH}}^2 = \frac{b_2^2}{6}N(N-1)(2N-1)\langle \delta\Omega^2 \rangle + N\langle \delta T^2 \rangle. \tag{43}$$

As expected, the leading term in timing jitter is due to SSFS and grows as N^5 whereas the GH term grows as N^3. Both of these contributions agrees with the earlier results of Essiambre and Agrawal [8]. The same expression applies for constant-dispersion fibers with minor changes. In particular, in the coefficients b_2 and b_3 L_{eff} are replaced with L_A because β_2 and β_3 are constant along the fiber. The parameter b_R remains the same but coefficient b_{2R} changes to $4\gamma T_R(L_{\text{eff}} - L_A)/\left(15\alpha\tau_0^3\right)$.

VI. Timing Jitter for CRZ Systems

In CRZ systems, input pulses are often prechirped but they do not follow a periodic evolution pattern. In general, the chirp and the pulsewidth cannot be calculated analytically because of the nonlinear effects. However, in quasi-linear links in which the GVD of each fiber section is so large that the pulse spreads over several bit slots, the pulse evolution is nearly linear along the DM link. The chirp and the pulsewidth of the pulses as a function of distance can then be found analytically [1]. Since the CRZ system is not periodic, C and τ have different values at different amplifiers. This feature complicates the calculation somewhat, but the procedure is straightforward. At the ith amplifier, the chirp and the pulsewidth are given by

$$C_i = C_0 + \frac{ib_2}{\tau_m^2} \tag{44}$$

$$\tau_i^2 = \tau_m^2\left(1 + C_0^2\right) + 2iC_0 b_2 + \frac{i^2 b_2^2}{\tau_m^2} \tag{45}$$

where τ_m is the minimum pulsewidth related to the input width of the chirped pulse through $\tau_0^2 = \tau_m^2\left(1 + C_0^2\right)$. When these equations are used in (11)–(13) together with $E_i = E_0$, a problem is encountered for terms with τ_i in the denominator. We solve this problem by assuming that the average dispersion over each amplifier spacing is small enough that the pulsewidth does not change much between two amplifiers. This is often the case in practice. By expanding τ_i^{-1} in a Taylor series in (11) and (12), the moments and variances are approximately given by

$$\left\langle \delta E_i^2 \right\rangle = 2SE_0,$$

$$\langle \delta\Omega_i \delta E_i \rangle = \frac{2S}{\sqrt{\pi}\tau_m\left(1 + C_0^2\right)^{1/2}}\left[C_0 - \frac{ib_2}{\tau_m^2}\left(1 + 2C_0^2\right)\right] \tag{46}$$

$$\left\langle \delta\Omega_i^2 \right\rangle = \frac{S(1 + C_0^2)}{E_0\tau_0^2}, \quad \langle \delta\Omega_i \delta T_i \rangle = \frac{S}{E_0}\left(C_0 + \frac{ib_2}{\tau_m^2}\right) \tag{47}$$

$$\left\langle \delta T_i^2 \right\rangle = \frac{S}{E_0}\tau_m^2\left[\left(1 + C_0^2\right) + \frac{2iC_0 b_2}{\tau_m^2} + \frac{i^2 b_2^2}{\tau_m^4}\right]$$

$$\langle \delta E_i \delta T_i \rangle = 0. \tag{48}$$

The timing jitter can now be calculated from (22)–(24) following the procedure outlined earlier. The result is given by

$$\sigma_t^2 = \sigma_{\rm GH}^2 + R_1 \left\langle (\delta E)^2 \right\rangle + \frac{2S}{\sqrt{\pi}\tau_m}(1+C_0^2)^{-1/2} \times \left[R_2' C_0 - \frac{R_2'' b_2}{\tau_m^2}\left(1+2C_0^2\right)\right] + \frac{R_3' S}{E} \quad (49)$$

where $\sigma_{\rm GH}$ is the GH contribution to the timing jitter and is given by

$$\sigma_{\rm GH}^2 = \frac{S\tau_m^2}{E} N \left[1 + \left(C_0 + \frac{b_2 N}{\tau_m^2} \right)^2 \right] \quad (50)$$

and the quantities R_2', R_2'', and R_3' are defined as

$$R_2' = N(N-1)b_2 \left[\frac{b_2 b_R (N-1)^2}{3} + \frac{b_{2R}(2N-1)}{3} \right] \quad (51)$$

$$R_2'' = N(N-1)\frac{b_2}{18} \times \left[\frac{b_2 b_R (12N^3 - 40N^2 - 53)}{10} + b_{2R}(9N^2 - 3N - 13) \right] \quad (52)$$

$$R_3' = N(N-1)b_3 \times \left[\frac{b_3(N-1)(N-2)}{6} + \frac{4b_2}{3\tau_m}\left(1+C_0^2\right)^{-1/2} \times \left(\frac{C_0}{2} - (2N-1)\left(1+2C_0^2\right)\frac{b_2}{3\tau_m^2} \right) \right]. \quad (53)$$

Because of the dependence of chirp and pulsewidth on distance, the contribution of R_2'' grows as N^5 as well. When the Raman effect and TOD are absent, we recover the expression for GH jitter for CRZ systems obtained in our earlier paper [10].

VII. Results and Discussion

The analytic expressions for the timing jitter obtained in this paper are based on the variational and moment methods and assume a specific pulse shape is maintained during propagation of the pulse. Before using them, we compare their prediction with the results obtained numerically by solving the NLS equation (1) while adding the noise at each amplifier. We use the well-known split-step Fourier method for this purpose [4] and launch a 32-bit pseudorandom bit sequence into the fiber link. Timing jitter is calculated by performing the integral in (1) over the bit slot of each 1 bit. To collect a large enough sample for the timing-jitter values, the NLS equation was solved repeatedly.

We first consider a 10-Gb/s dispersion-managed system. The dispersion map consists of 10.5 km of anomalous-GVD fiber with $D = 4$ ps/(km-nm) and 9.7 km of normal-GVD fiber with $D = -4$ ps/(km-nm). Each fiber section has 0.2-dB/km losses and a nonlinear parameter $\gamma = 1.7$ W$-$1/km. The amplifiers spacing is 80.8 km. The spectral noise density was calculated using $n_{sp} = 1.3$. The input-pulse parameters were found using the periodicity conditions for solitons and have values $\tau_0 = 12$ ps, $C_0 = 0.52$, and $E_0 = 0.03$ pJ. The pulsewidth [full-width at half-maximum (FWHM)] of about 20 ps needed for the 10-Gb/s system is large enough that the contribution of Raman jitter is expected to be negligible. This is indeed found to be the case. Fig. 1 shows the timing jitter obtained numerically (shown by asterisks) and compares it with the results obtained using (27). The agreement is quite reasonable and justifies our use of the variational and moment methods.

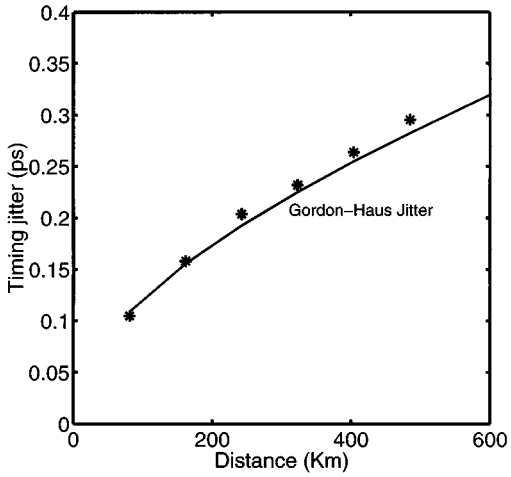

Fig. 1. Timing jitter for a 10-Gb/s DM soliton system with 80.8-km amplifier spacing. The solid line shows the analytical prediction of the moment theory while the asterisks show the numerical values obtained by solving the NLS equation. The dispersion map is such that $\beta_{av} \approx -0.2$ ps^2/km.

To include the Raman jitter, we next consider a dispersion-managed system capable of operating at 160 Gb/s. The use of dense dispersion-management is essential at such high bit rates [17]. The dispersion map consists of 1.0 km of anomalous-GVD fiber with $D = 2.5$ps/(km·nm) and 1.0 km of normal GVD fiber with $D = -2.35$ps/(km·nm). All other parameters remain the same. We also need the values for T_R and β_3; we choose $T_R = 3$ fs and $\beta_3 = 0.1$ ps^3/km. Optical amplifiers are spaced 40 km apart for this system. The input-pulse parameters were again found using the periodicity condition and have values $\tau_0 = 1.25$ ps, $C_0 = 1$, and $E_0 = 0.12$ pJ. The FWHM of the pulse is only about 2 ps because of the 6.25-ps bit slot at 160 Gb/s. This feature makes the Raman effect important enough that we expect it to dominate the jitter. We compare the analytical results obtained using (26) to the results of numerical simulation (stars) in Fig. 2. Notice the rapid growth of the jitter because of the Raman contribution to the total timing jitter. The numerical values are somewhat larger compared with the predicted values. We attribute this discrepancy to the jitter induced by the intrachannel effects that are not include in our analysis but are automatically included in the numerical simulations. This fact should be kept in mind.

We now use our analytic results to study the role of the Raman and TOD effects. All of the following results are for a 160-Gb/s DM system using the same map that was used for Fig. 2. Fig. 3 shows the the timing jitter for the DM-soliton case as a function of distance. The dashed line show the contribution of GH jitter, while the solid line adds the contribution of the Raman jitter. Solid dots are obtained when the effects of TOD are also included. The most important conclusion one can draw from Fig. 3 is that the Raman contribution begins to dominate after a distance of 400 km (ten amplifier spacings) because of its N^5 dependence on the number of amplifiers but the TOD contribution is negligible. Since the Raman contribution dominates the jitter after 500 km, the system performance is likely to be limited by the Raman-induced frequency shift at high bit rates.

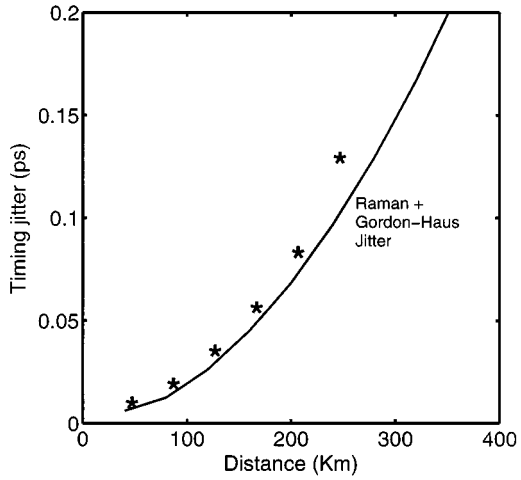

Fig. 2. Same as in Fig. 1 except that bit rate is increased to 160 Gb/s and amplifier spacing is reduced to 40 km. A dense dispersion map (map period 2 km) is used with $\beta_{av} = -0.1$ ps^2/km. The Raman contribution becomes quite important at such high bit rates.

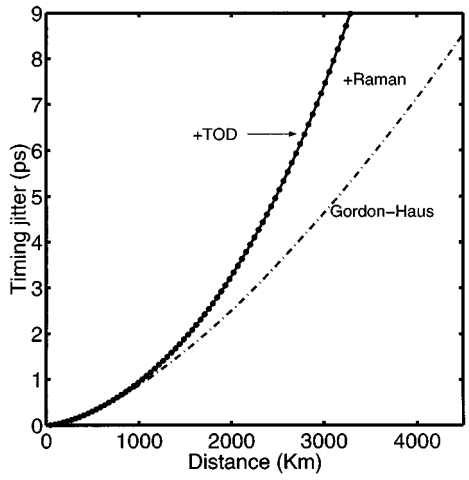

Fig. 4. Timing jitter for a 160-Gb/s soliton system based on DDFs with amplifiers spaced 45-km apart. The dot-dashed line shows the Gordon–Haus contribution alone while the solid line adds the Raman contribution. The filled circles include the TOD effects. The average dispersion is -1.275 ps^2/km.

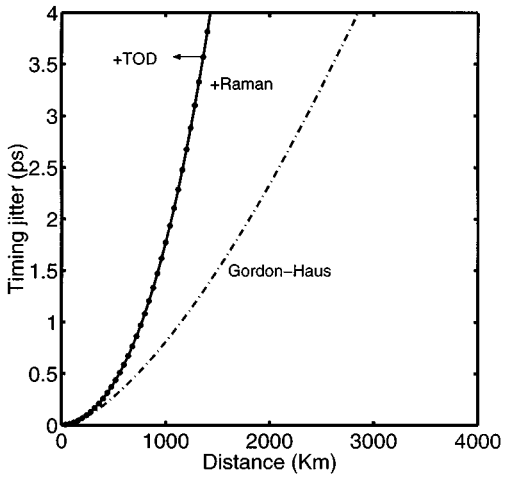

Fig. 3. Timing jitter for the 160-Gb/s DM solitons system with the map used for Fig. 2. The dot-dashed line shows the GH contribution alone while the solid line adds the Raman contribution. The filled circles include the TOD effects.

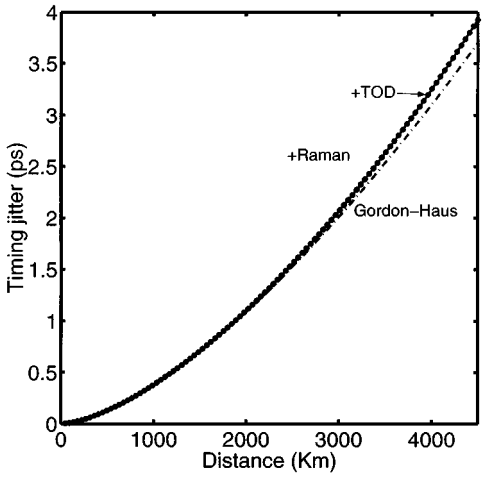

Fig. 5. Same as in Fig. 4 except that the avearge dispersion has been reduced to -0.1 ps^2/km for comparison with the case of DM solitons.

One may wonder whether the DDFs will help in reducing the Raman jitter. We consider the 160-Gb/s soliton system again but replace the dispersion map with a 45-km-long DDF with $D(0) = 1.0$ps/(km·nm). All other parameter remain the same but the input pulse energy was set to 0.9 pJ so that it corresponds to a standard fundamental soliton. Fig. 4 shows the dependence of timing jitter on distance for such a system. The dashed line shows the GH jitter obtained from (43), the solid line adds the contribution of the Raman jitter from (42), and solid dots include the effect of TOD as well. Notice that the timing jitter is much larger for DDFs compared with the case of DM solitons. This is due to a relatively large value of the average dispersion. If we design the standard soliton system with the same average dispersion using a DDFs whose $|\beta_2|$ decreases from 0.24 to 0.03 ps^2/km over 45 km (required pulse energy of 0.17 pJ), we obtain the results shown in Fig. 5. Timing jitter is now smaller than that for DM solitons shown in Fig. 3. This qualitative change is due to different energy dependence for the Raman and GH jitters. The Raman jitter has its origin in energy fluctuations whose magnitude is proportional to the pulse energy. In contrast, the GH jitter is inversely proportional to the pulse energy. Thus, as the pulse energy decreases, the GH jitter increases but the Raman jitter decreases.

Finally, we consider timing jitter in CRZ systems using the same dense dispersion map used for Fig. 2. The pulse energy was reduced by a factor of ten compared with the case of DM solitons to weaken the nonlinear effects. The average dispersion was also lowered to $\beta_{av} = -0.05$ ps^2/km by changing β_2 of the normal GVD section of the map. The input chirp C_0 was chosen to be equal to $|\beta_2|L/\tau_m^2$, where L is the total distance of propagation, so that the pulse is unchirped at the output end. Fig. 6 shows how timing jitter varies as a function of distance. The dashed line shows the GH jitter expected in the absence of the Raman contribution $(T_R \approx 0)$. This component of the timing jitter first increases and then decreases because of precompensation of the GVD . This behavior was predicted in our earlier paper [10]. The solid line adds the Raman contribution while the filled circles show the total jitter with the TOD effects included. Again, the TOD effects are negligible. The Raman jitter

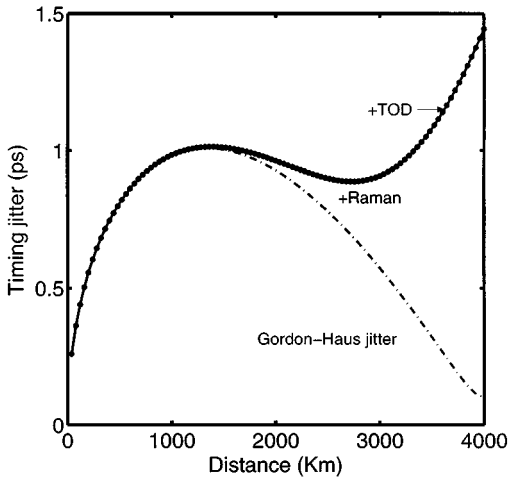

Fig. 6. Timing jitter for a quasilinear 160-Gb/s CRZ system for the same dispersion map as in Fig. 3, but for pulses with 10 times reduced energy. The average dispersion was reduced to -0.05 ps^2/km. The dot-dashed line shows the Gordon–Haus contribution alone while the solid line adds the Raman contribution. The effects of TOD remain negligible unless average dispersion is close to zero.

dominates after 2000 km in this case, but can be reduced by reducing the average dispersion of the system. The ideal case corresponds to $\beta_{av} = 0$ because only the linear term is then left in the timing-jitter expression. The effects due to TOD will then become dominant.

VIII. Summary

In this paper, we have presented an analytic theory of Raman-induced timing jitter for high-speed dispersion-managed lightwave systems using the moment method. The input pulse is assumed to maintain its original Gaussian shape, but its amplitude, width, chirp, position, and frequency are allowed to evolve along the fiber link. Our analysis can be used in the case of dense dispersion management, realized using multiple map periods between two neighboring amplifiers. We have included the effects of third-order dispersion as well in this paper. We have checked the accuracy of our approximations by solving the NLS equation using the split-step Fourier method.

We have applied the general formalism to three types of lightwave systems corresponding to the use of DM solitons, standard solitons with DDFs, and CRZ pulses in a quasilinear configuration. We were able to obtain simple analytic expressions for the timing jitter in each case. We compared the three configurations for a 160-Gb/s system and found that Raman-jitter variance increases with the number N of amplifiers as N^5. The Raman jitter begins to dominate after a few hundred kilometers $(N \sim 10)$ in the case of DM solitons. In the case of standard solitons propagating inside DDFs, the Raman contribution is smaller because of the reduced pulse energy but the total jitter is quite large. In the case of quasi-linear CRZ systems, the Raman jitter dominates at large distances (above 2000 km in Fig. 6), but can be reduced by lowering the average value of the dispersion so that it is close to zero. In all cases, jitter can exceed the acceptable value (about 0.5 ps at 160 Gb/s) after 500 km or so, indicating that such systems cannot be operated over long distances unless a jitter-reduction scheme is implemented. The use of parametric amplifiers is likely to be beneficial in this context [18].

References

[1] G. P. Agrawal, *Fiber-Optic Communication Systems*, 3rd ed. New York: Wiley, 2002.
[2] E. Iannone, F. Matera, A. Mecozzi, and M. Settembre, *Nonlinear Optical Communication Networks*. New York: Wiley, 1998, ch. 5.
[3] G. P. Agrawal, *Applications of Nonlinear Fiber Optics*. San Diego, CA: Academic, 2001.
[4] ——, *Nonlinear Fiber Optics*, 3rd ed. San Diego, CA: Academic, 2001.
[5] J. P. Gordon and H. A. Haus, "Random walk of coherently amplified solitons in optical fiber transmission," *Opt. Lett.*, vol. 11, pp. 665–667, 1986.
[6] J. P. Gordon, "The theory of soliton self-frequency shift," *Opt. Lett.*, vol. 11, pp. 662–664, 1986.
[7] D.-M. Baboiu, D. Mihalache, and N.-C. Panoiu, "Combined influence of amplifier noise and intrapulse Raman scattering on the bit-rate limit of optical fiber communication systems," *Opt. Lett.*, vol. 20, pp. 1865–1867, 1995.
[8] R. J. Essiambre and G. P. Agrawal, "Timing jitter of ultrashort solitons in high-speed communication systems. I. General formulation and application to dispersion-decreasing fibers," *J. Opt. Soc. Amer. B*, vol. 14, pp. 314–322, 1997.
[9] V. S. Grigoryan, C. R. Menyuk, and R. M. Mu, "Calculation of timing and amplitude jitter in dispersion-managed optical fiber communications using linearization," *J. Lightwave Technol.*, vol. 17, pp. 1347–1356, Aug. 1999.
[10] J. Santhanam, C. J. McKinstrie, T. I. Lakoba, and G. P. Agrawal, "Effects of precompensation and post-compensation on timing jitter in dispersion-managed systems," *Opt. Lett.*, vol. 26, pp. 1131–1133, 2001.
[11] C. J. McKinstrie, J. Santhanam, and G. P. Agrawal, "Gordon–Haus timing jitter in dispersion-managed systems with lumped amplification: Analytical approach," *J. Opt. Soc. Amer. B*, vol. 19, May 2002.
[12] E. Poutrina and G. P. Agrawal, "Effect of distributed Raman amplification on timing jitter in dispersion-managed lightwave systems," *IEEE Photon. Technol. Lett.*, vol. 14, pp. 39–40, Jan. 2002.
[13] S. K. Turitsyn, I. Gabitov, E. W. Laedke, V. K. Mezentsev, S. L. Musher, E. G. Shapiro, T. Schafer, and K. H. Spatschek, "Variational approach to optical pulse propagation in dispersion compensated transmission systems," *Opt. Commun.*, vol. 151, pp. 117–135, 1998.
[14] A. Berntson, N. J. Doran, W. Forysiak, and J. H. B. Nijhof, "Power dependence of dispersion-managed solitons for anomalous, zero, and normal path-average dispersion," *Opt. Lett.*, vol. 23, pp. 900–902, 1998.
[15] T. I. Lakoba, J. Yang, D. J. Kaup, and B. A. Malomed, "Conditions for stationary pulse propagation in the strong dispersion management regime," *Opt. Commun.*, vol. 149, pp. 366–375, 1998.
[16] T. I. Lakoba and D. J. Kaup, "Influence of the Raman effect on dispersion-managed solitons and their interchannel collisions," *Opt. Lett.*, vol. 24, pp. 808–810, 1999.
[17] A. H. Liang, H. Toda, and A. Hasegawa, "High-speed soliton transmission in dense periodic fibers," *J. Opt. Soc. Amer. B*, vol. 24, pp. 798–801, 1999.
[18] R. J. Essiambre and G. P. Agrawal, "Timing jitter of ultrashort solitons in high-speed communication systems. II. Control of jitter by periodic optical phase conjugation," *J. Opt. Soc. Amer. B*, vol. 14, pp. 323–330, 1997.

Jayanthi Santhanam received the B.S. degree from Sri Satya Sai Institute of Higher Learning, Anantapur, India, and the M.S. degree from the Indian Institute of Technology, Madras, India. She is working toward the Ph.D. degree in physics at the University of Rochester, Rochester, NY.

Her research interest includes timing jitter in dispersion-managed communication systems.

Govind P. Agrawal (M'83–SM'86–F'96) received the B.S. degree from the University of Lucknow and the M.S. and Ph.D. degrees from the Indian Institute of Technology, New Delhi, India, in 1969, 1971, and 1974, respectively.

After holding positions at the Ecole Polytechnique, France, the City University of New York, New York, and AT&T Bell Laboratories, Murray Hill, NJ, he joined the faculty of the Institute of Optics at the University of Rochester where he is a professor of optics, in 1989. His research interests focus on quantum electronics, nonlinear optics, and laser physics. In particular, he has contributed significantly to the fields of semiconductor lasers, nonlinear fiber optics, and optical communications. He is an author or coauthor of more than 300 research papers, several book chapters and review articles, and four books.

Dr. Agrawal is a Fellow of the Optical Society of America (OSA). He has participated many times in organizing the technical conferences sponsored by the OSA and the IEEE. He was the program cochair in 1999 and the general cochair in 2001 for the Quantum Electronics and Laser Science Conference. He also chaired a program subcommittee for the Nonlinear Guided Waves and their Applications Conference, in 2001.